Submitted to *Geophysical Review Letters*, December 2023, Revised February 2024

Atmospheric Escape from Earth and Mars: Solar and Solar Wind Drivers of Oxygen Escape

W.K. Peterson[1], D.A. Brain[1], N.R. Schnepf[1], Y. Dong[1], P. Chamberlin[1], and A.W. Yau[2]

[1]LASP, University of Colorado Boulder
[2]University of Calgary, Canada

Key points:

- We derive oxygen escape rates from Earth as a function of solar wind parameters from a reanalysis of Dynamics Explorer 1 data.
- O^+ escape from Earth varies by a factor of 2 as a function of the solar wind magnetic field component aligned with the Earth's field.
- Oxygen escape rates from Mars are not as sensitive to variations in the solar power components as those from Earth.

Index Terms:

2756 Planetary magnetospheres (5443, 5737, 6033)
2784 Solar wind/magnetosphere interactions
2479 Solar radiation and cosmic ray effects
2162 Solar cycle variations (7536)

Keywords:

Atmospheric escape, Terrestrial planets, solar wind energy, solar irradiance, Mars, Earth

Abstract:

Habitability at the surface of a planet depends on having an atmosphere long enough for life to develop. The loss of atmosphere to space is an important component in assessing planetary surface habitability. Current models of atmospheric escape from exoplanets are not well constrained by observations. Atmospheric escape observations from the terrestrial planets are available in public data archives. We derive oxygen escape rates from Earth as a function of solar wind parameters from a reanalysis of Dynamics Explorer 1 data and compare them to similar data from Mars. The reanalyzed Earth data are consistent with prior reports of escape from Earth as a function of geomagnetic indices. The reanalysis shows a dependence on the angle between the solar wind magnetic field and the Earth's magnetic field. It also demonstrates that oxygen escape rates from Mars are not as sensitive to variations in solar power components as those from Earth.

Plain Language Summary

Habitability of a planet depends on having an atmosphere long enough for life to develop. NASA and ESA data archives contain information about atmospheric escape from the terrestrial planets. For these planets oxygen ions dominate atmospheric escape. The data archives are just beginning to be analyzed and presented in a form that allows comparison with, and validation of, models of the interaction of stellar winds with exoplanets. We derive oxygen escape rates from Earth as a function of solar power components from a reanalysis of Dynamics Explorer 1 data and compare them to similar data from Mars. Our analysis demonstrates that oxygen escape rates from Mars are not as sensitive to variations in the solar power components as those from Earth. These data and similar data from Venus will prove to be important constrains on models of stelar wind/atmosphere interactions and atmospheric escape from exoplanets.

1 Introduction:

The ability of a planet to retain an atmosphere influences whether water can be stable as a liquid at the planet's surface. Understanding the evolution of planetary atmospheres requires knowledge of atmospheric escape for different star and planet combinations. A planet's atmospheric state is the result of source, loss, and modification processes that have acted on the atmosphere over time. The loss of atmosphere to space is an important component in assessing planetary surface habitability. Shizgal and Arkos (1996) reviewed the processes responsible for atmospheric loss from terrestrial planetary atmospheres and concluded: "The main mechanism for loss of atmospheric constituents appears to be the ionization of the neutral atmosphere by photoionization …". Recently Cravens et al. (2017), Gunell et al., (2018), and others have suggested that dissociative recombination could produce significant escape of neutral oxygen from Mars.

Escaping oxygen ion observations are available from the terrestrial planets. Recent reviews of observations and models of escaping ions at Mars (Brain et al. 2017), Venus (Persson et al. 2020) and Earth (Welling et al., 2015 and Yau et al. 2021) have elucidated the important role of induced (Venus and Mars) or intrinsic planetary-scale (Earth) magnetic fields in ion escape. Strangeway et al. (2010) first raised the question "Does a planetary-scale magnetic field enhance or inhibit ionospheric plasma escape?" Based on comparisons of total escape rates measured on Earth, Mars, and Venus, Strangeway et al. (2019) concluded that a planetary-scale magnetic field could enhance ionospheric escape. Gunell et al. (2018) and Ramstad and Barabash (2021) have reviewed oxygen loss measurements made at Mars, Venus, and Earth as a function of solar photoionizing flux and solar wind dynamic pressure and reached the same conclusion. Solar energy inputs, however, are not completely described by the solar wind pressure and the intensity of the ionizing radiation.

Not only are the magnetic environments of the terrestrial planets different; the magnitude of solar energy inputs to their atmospheres driving ion escape vary widely. Ion escape is powered by solar energy. This energy includes ionizing radiation directly from the Sun as well as kinetic and electromagnetic energy carried in the solar wind.

The direct solar electromagnetic radiation below 90 nm ionizes the neutral atmosphere to produce the ionosphere from which ions escape. The importance of solar extreme ultraviolet radiation below 90 nm (EUV) and its variation parameterized by the solar $F_{10.7}$ index in driving heavy ion escape is well established for Earth (e.g. Yau et al 1985, 1988, 2021). The relative importance of solar wind electromagnetic and kinetic energy in driving atmospheric escape is not well established. Recently Lockwood (2019) determined that the solar wind electromagnetic flux provides ~10% of the power input to the Earth's magnetosphere and argues that it contributes to the plasma processes that drive geomagnetic activity and consequent ion escape.

Measurements of the solar wind electromagnetic energy flux, i.e. the Poynting flux (S) and kinetic energy flux (K) have been available from solar wind monitors since 1970 (Feldman et al. 1978). These solar wind data were initially difficult to obtain and use so early Earth investigators focused on ground based geomagnetic indices such as K_P, D_{ST}, and A_E which parameterize solar geomagnetic activity driven by changes in solar energy inputs (e.g. Yau et al. 1988). More recently investigators have begun to parameterize atmospheric escape as a function of a single component of solar wind energy: the solar wind dynamic pressure (e.g. Ramstad and Barabash, 2021). Shillings et al. (2019) have reported escape fluxes as a function of coupling parameters that include elements used to calculate the Poynting flux. Earth-centric coupling parameters are not applicable to Mars. To our knowledge atmospheric escape has only been measured as a function of both solar wind electromagnetic and kinetic energy fluxes incident on Earth's magnetosphere by Lennartsson et al. (2004) and at Mars by Schnepf et al. (2024).

Lennartsson et al., (2004) hereafter called Lenn04 reported energetic H^+ and O^+ escape rates from the Earth's magnetosphere using data from NASA's Polar satellite for three years (1996-1998) during a solar minimum period as a function of Poynting flux (S) and solar wind kinetic energy flux (K). The data were further sorted for intervals where the solar wind magnetic field was parallel or anti-parallel to Earth's magnetic field. Data sampling limitations precluded an analysis of the escape rates as a function of solar ionizing radiation. They found increasing O^+ escape rates with increasing S and K intensity for both orientations of the solar wind magnetic field. The limited number of intervals where both escaping ion observations from the Polar satellite and solar wind data were simultaneously available compounded with the lack of data from a solar maximum interval limited the conclusions that could be drawn from the data.

Our ultimate objective is to use escaping oxygen observations from terrestrial planets to partially validate models attempting to describe atmospheric loss from planets of other stars. Progress in understanding the influence of solar energy inputs on the ion escape from terrestrial planets requires comprehensive observations of all input power sources and escaping ion fluxes from each planet. A first step in this process is to use archived solar wind and escaping ion data at Earth to expand the data base of escaping ions as a function of all solar drivers: solar ionizing radiation, Poynting flux (S) and kinetic energy flux (K) at Earth.

2 Data:

The ion data we use to calculate escape rates are from the Energetic Ion Mass Spectrometer (EICS, Shelley et al. 1981) on the Dynamics Explorer 1 satellite (DE 1, Hoffman and Schmerling, 1981) acquired from September 1981 to February 1991 spanning Cycle 21 and 22. We use archived hourly average solar wind parameters from the IMP-8 satellite to calculate the solar wind power components S and K as well as the solar wind magnetic field direction. A model of the daily solar spectrum (Chamberlin et al. 2020) is integrated over two wavelength ranges to obtain measures of the solar ionizing radiation power: Q_{EUV} (0-45nm) and I_{EUV} (0-90 nm).

2.1 Dynamics Explorer 1

The DE 1 orbit has an apogee of 23,000 km, a perigee of 570 km and an inclination of 90°. Its orbital plane has a local time drift period of 12 months and a line-of-apsides drift period of 18 months. 96-s cadence O^+ flux and 1 sigma uncertainty based on the number of samples in 15 broad energy bins sensitive to energies from 10 eV/q to 20 keV/q and 14 pitch angle bins in NASA's CDF format were acquired and processed. Each interval was characterized by five data quality flags. Only the highest quality data acquired above 6,000 km were used. Data for each 96s interval were normalized to an altitude of 300 km and binned into 12 magnetic local time (MLT) and 16 Invariant latitude (INVL) bins.

2.2 IMP 8

Selected one hour resolution solar wind parameters from the Interplanetary Monitoring Platform 8 (IMP 8, Feldman et al. 1978 and references therein) were obtained and processed. Specifically, we used the solar wind kinetic energy flux density (K) and the solar wind electromagnetic energy flux density (S, Poynting flux)

$$K = \frac{1}{2}(M_h N_h + M_{he} N_{he})V^3 \quad (1)$$
$$S = VB^2 \cos^2\Theta/\mu_0 \quad (2)$$

where Mh and Mhe are the H^+ and He^{++} atomic mass, Nh and Nhe the H^+, and He^{++} number density, V the solar wind velocity, B the IMF magnitude and θ the angle between the solar wind velocity and magnetic field (Maggiolo et al, 2022). μ_0 is the magnetic permeability of free space. One-hour resolution magnetic field data in GSM coordinates were used to calculate the IMF clock and cone angles. The clock angle is the projection of the magnetic vector onto the B_Y B_Z plane. The cone angle is the projection of the magnetic vector onto the B_X B_Y plane.

The IMP 8 satellite had a 30 R_E orbit and so is often in the magnetosphere where reliable calculations of solar wind K and S are impossible. There is a magnetospheric flag included in the NASA data set indicating when IMP 8 is not in the magnetosphere. Unfortunately, the magnetospheric flag is not available after Jan 1, 1988. We selected only data where the magnetospheric flag was 6 or greater indicating the highest quality S and K values. Following Lenn04, parameters obtained from the IMP 8 satellite were time shifted 15 minutes to account for solar wind travel time to the magnetosphere.

2.3 Solar Ionizing Radiation

The $F_{10.7}$ radio flux has been a standard proxy for solar EUV irradiance due to its ease of ground-based measurements and the long historical daily dataset ranging back to 1947. More recent studies have shown the break in the $F_{10.7}$ index and EUV irradiance relationship, especially for higher solar activity (Schonfeld et al., 2015, 2019). This is due to the $F_{10.7}$ solar radio flux being comprised of two distinct formation mechanisms, namely the bremsstrahlung radiation, which does correlate well with EUV irradiance, and the gyromagnetic radiation, which has no relation to the EUV irradiance; therefore, the $F_{10.7}$ index is not a pure measurement of solar EUV irradiance and fails to accurately represent its variability at times when dominated by the second component.

Rather than using the solar $F_{10.7}$ index to parameterize the rates of escaping oxygen ions, use integrals of the solar irradiance spectrum over two different wavelength ranges. Daily estimates of the solar irradiance spectrum at 1-nm resolution below 190 nm are available from the Flare Irradiance Spectral Model Version 2 (FISM2, Chamberlin et al. 2020). This model uses a combination of observations and solar indices to construct daily average solar spectra (0-190 nm) from 1947 to present.

We use the integral over the spectral range that produces ionization in the atmosphere (i.e. below 90 nm) and designate it I_{EUV}. Schnepf et al. (2024), Dong et al. (2023) and others have used this index to parameterize oxygen ion escape from Mars.

We also use an integral over the wavelength range that produces photoelectrons that in turn ionize neutral constituents of the upper atmosphere. The integral of the solar spectrum below 45 nm is identified as Q_{EUV}. Strickland et al. (2004) and Meier et al. (2015) demonstrated that Q_{EUV} values determined a from integrating solar spectra agreed well with those determined from remote sensing of the O/N_2 ratio in Earth's airglow.

2.4 Data Processing

Data from DE 1 and IMP 8 are not continuous. There are 348,281 intervals with high quality DE 1 observations above 6,000 km. Of these 70,568 have simultaneous IMP 8 observations suitable for calculating S and K. Figure 1 panels A, B, and C display respectively the input, intermediate, and final data. Figure 1B shows how the individual DE 1 escaping O^+ observations normalized to 300 km are binned in 14 INVL bins between 58 and 90 degrees and 12 two-hour MLT bins. The software calculating INVL available at the time the DE 1 data were archived did not return INVL values greater than 85°. Peterson et al. (2008) have shown that the net escapiing O^+ from the polar cap is negligible. Figure 1B shows that sampling in INVL/MLT space was non-uniform. The maximum and minimum number of samples in an individual bin were 2,389 and 83 respectively. Integrating the map of escaping O^+ fluxes in Figure 1B, and doubling it for the two hemispheres, gives $1.3 \times 10^{26} \pm 8.3 \times 10^{25}$ O^+ ions per second escaping the Earth. The escape rate is consistent with the results of Yau et al. (1988) who used a lower resolution, preliminary version of the EICS data.

To determine the variation in net O^+ escape rates as a function of solar energy inputs, the data shown in Figure 1B were further sub-divided into six S, K, $I_{EUV,}$ or Q_{EUV} INVL/MLT maps with approximately equal numbers of samples. This division provides optimum sampling and resolution for our purposes.

The O^+ escaping fluence and estimated uncertainty as a function of S, K, and Q_{EUV} shown in Figure 1C are obtained by projecting the fluence at each INVL/MLT bin for each map onto a spherical surface at 300 km altitude (6670 km geocentric radius) and then integrating over the surface. Median values of S, K, and Q_{EUV} for each of the six levels used in each map are shown in units of W/m^2. We note that if the escape rate were independent of S, K, or Q_{EUV} the escape rate would be constant and equal to 1.3×10^{26} ion/s obtained from the average map shown in Figure 1B. Figure 1C shows variations of O^+ escape with an increase of each of these variables. There appears to be a threshold value of the hourly average Poynting flux (S) above which it has an impact on O^+ escape. The O^+ escape rate appears to depend exponentially on the hourly average kinetic energy flux (K). The O^+ escape rate increases more rapidly at the lower values of $Q_{EUV.}$ The dependence of escaping O^+ as a function of I_{EUV} is almost identical to that of Q_{EUV} and not shown in Figure 1C.

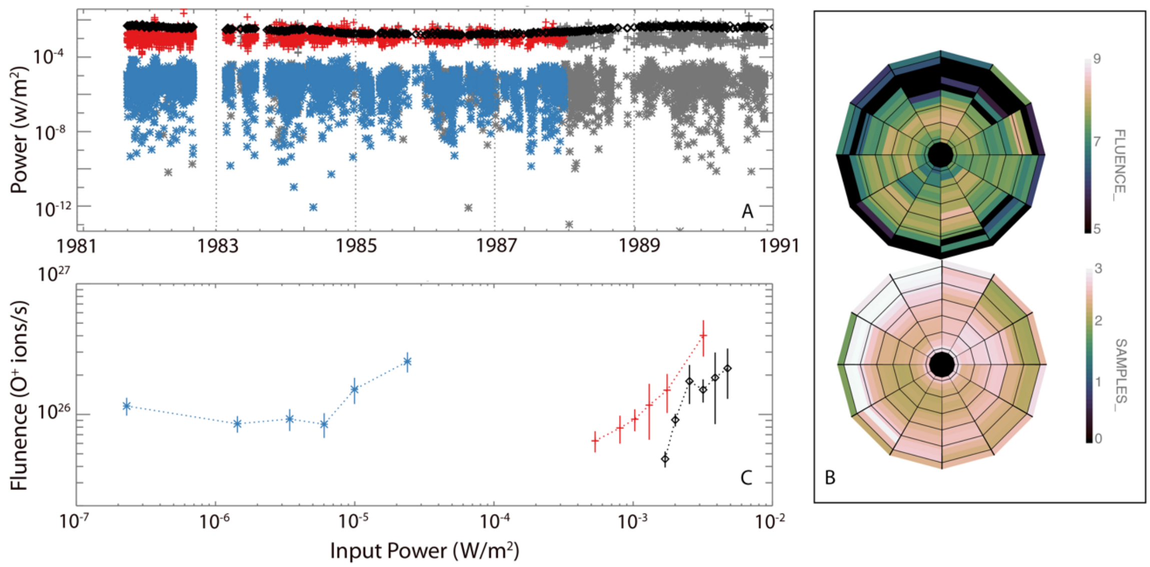

Figure 1. Input (A), intermediate (B) and final (C) data. Panel A: Input solar wind Poynting flux S indicated by * symbols and kinetic energy flux K indicated by + symbols. Intervals where high-quality S and K values are available are shown as blue and red symbols respectively; the other intervals are shown as grey symbols. Solar irradiance integral powers Q_{EUV} and I_{EUV} are show as black diamonds and X's respectively. Panel B: Top: DE 1 escaping O^+ fluxes in units of the logarithm of ions/cm^2-s normalized to 300 km are binned in 14 INVL bins between 58 and 90 degrees and 12 two-hour MLT bins. Bottom: logarithm of the number of data samples in each MLT-INVL bin. C: O^+ escaping fluence and estimated uncertainty as a function of S (*), K (+), and Q_{EUV} (diamond). Uncertainties are shown as vertical lines.

3 Discussion

We are interested in comparing ionospheric escape rates from the terrestrial planets as a function of all solar power inputs. NASA and ESA have supported multiple missions that have observed plasma escaping the terrestrial planets. The available data on oxygen ion escape rates as a function of all solar power inputs, however, is limited. Specifically, published data on the effect of variations in solar wind Poynting flux (S) on atmospheric escape is comprehensive for only Mars (Schnepf et al. 2024), partially available for Earth (Lenn04), and non-existent for Venus. Strangeway et al. (2005) and others have corelated outflowing ions with the locally measured Poynting flux. We do not use the Pointing flux observed at DE 1 which is different than that observed in the solar wind (Rodríguez-Zuluaga, et al. 2022)

Data obtained on the DE 1 satellite from NASA's archives have been reprocessed to produce estimates of the variation of O^+ escape from Earth as a function of components of solar power input. The results of this reanalysis are shown in Figure 1C which presents the rate of escaping O^+ as a function of S, K, and Q_{EUV}. The components of solar and solar wind power per unit area incident on the Earth and its magnetosphere vary over 5 orders of magnitude over the interval investigated. Q_{EUV} and I_{EUV} are used here to parameterize variations in the power input from solar ionizing radiation. I_{EUV} is included for comparison with the Mars data reported in Schnepf et al. (2024) and Dong et al. (2023). We note that the Schnepf et al., data in Figure 2E do not include data from the early mission which had the highest values of I_{EUV} included in the Dong et al. data.

The three components of incident power shown in Figure 1C have different entry paths to the magnetosphere and affect O^+ escape rate differently. The power in solar irradiance (Q_{EUV} and I_{EUV}) is transferred to the ionosphere below about 500km whereas the power in both K and S is transferred to a much larger area: i.e. the Earth's magnetopause at altitudes above about 60,000 km. The dependence of the ion escape is different for these parameters. Poynting Flux (S) appears to have a threshold value below which it has no effect on the oxygen escape rate. The oxygen escape rate as a function Q_{EUV} and I_{EUV} (not shown in Figure 1) has different rates of increase at low and high values of Q_{EUV} and I_{EUV}. In addition, the ratios of maximum to minimum escape rates over the Q_{EUV}, S, and K parameter ranges are different being 4.9, 3.0, and 6.4 respectively.

The Earth's large scale magnetic field has a strong influence on the paths available to incoming solar wind kinetic and electromagnetic energy fluxes. Lenn04 reported a factor of 2 variation of O^+ escape rates as a function of S and K for positive and negative values of IMF B_Z. The reprocessed DE 1 data have a similar dependence on IMF B_Z as shown below.

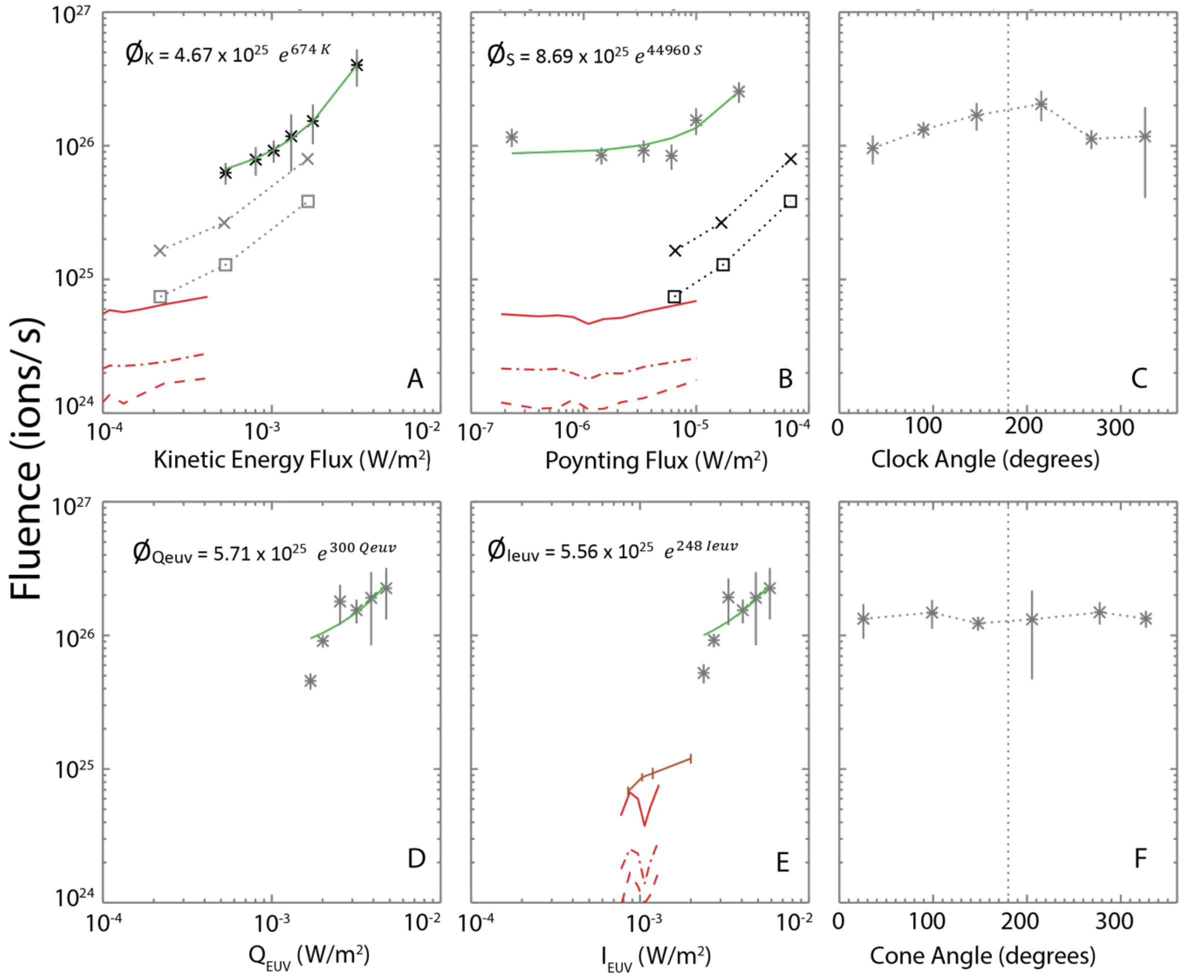

Figure 2. Escaping Earth oxygen rates as a function of S, K, Solar wind clock angle, Q_{EUV}, I_{EUV}, and solar wind cone angle from this analysis, Schnepf et al. (2024), Dong et al. (2023), and Lenn04. Data from Earth are shown in black and green lines and symbols; data from Mars are shown in red and brown. Data from this analysis are shown as stars with associated uncertainties shown as vertical lines. Exponential fits to the data are shown as solid green lines with parameters of the fit in the upper left of the panel. The Mars data reported by Schnepf et al. are shown in panels A, B, and E as red lines: O^+ as dashed lines, O_2^+ as dot dashed lines and total O as a solid line. The Mars total oxygen escape data from Dong et al. (2023) are shown in Panel E as a brown line with vertical red bars indicating the uncertainty. Apogee data above 50,000 km from Lenn04 are reported in panels A and B as X and box symbols. Intervals where Bz is strongly southward ($B_Z < -3$nT) are encoded by X symbols. Intervals where B_Z is strongly northward ($B_Z > 3$ nT) are encoded by box symbols. Earth O^+ escape rates as a function of solar wind clock and cone angles are presented in panels C and F.

Figure 2 presents O^+ escape rates as a function of K, S, Q_{EUV}, I_{EUV}, IMF clock and cone angle. These data are compared and contrasted with available observations from Earth and Mars. Panels C and F show that the average oxygen escape rate varies only as a function of one component of the solar wind magnetic field, the component aligned with the Earth's magnetic field, B_Z. Panel C shows that the peak escaping flux is near a cone angle of 180^o (B_Z negative, B_Y near 0) a factor of 2.1 greater than the minimum near 0^o, consistent with Lenn04. It is well known that geomagnetic activity is strongly dependent on the direction and intensity of the interplanetary magnetic field (IMF) relative to the Earth's dipole axis (Bz). Masunaga et al. (2013) have shown that the escape of oxygen from Venus does not depend on the IMF magnetic field direction. Dong et al. (2015, 2023), Schnepf et al. (2024) and others have shown that oxygen escape from Mars is best organized in Mars Solar Electric (MSE) coordinates defined by the solar wind electric field (-V x B) which is perpendicular to both the solar wind velocity and magnetic field. There are no observations of variations in oxygen escape from Mars as a function of the IMF magnetic field direction relative to any Martian geographic or magnetic direction nor is such a dependence expected. The data presented here affirm the conclusions of Gunnel et al. (2018), Strangeway et al. (2019), and Ramstad and Barabash (2021) that a planetary-scale magnetic field enhances ionospheric escape.

The range of K and S values sampled in Lenn04 shown in panels A and B differ from the ones sampled in the DE 1 data and reported here. Maggiolo et al. (2022) report one-hour average values for S and K obtained from the NASA archives. The variability of S and K in the 1996-1998 interval investigated by Lenn04 is greater than that in the 1981-1991 interval reported here. Lenn04 reported values when K values were about ½ and S values about 2 times those reported in Figures 1C and 2A and B. The Lenn04 analysis was based on 15-minute average S and K values rather than the 1-hour values considered here. We conclude that sampling biases introduced by the limited intervals for which O^+ escaping fluxes and solar wind S and K values were available are major contributors to the higher values of S and lower values of K sampled by Lenn04.

Cully et al., (2003) noted that differences in the magnitude of estimated escape rates arise from many factors including differences in altitude and energy range sampled. The difference between the magnitudes of the average total O^+ escape rates from DE1 and Polar in panels A and B are consistent with the analyses presented in Peterson et al., (2006) and Lenn04..

For analysis of the dependence on S and K Lenn04 considered only intervals with extreme values of the B_Z direction. In Figure 2B, there appears to be a threshold power of 2 x 10^{-6} W/m^2 below which the escape rate is constant in the DE 1 data. The rate of increase in O^+ escape as a function of S above this value is similar for both the DE 1 data reanalyzed here and the values reported in Lenn04. Because of limited data, Lenn04 was forced to calculate total escape in only three S ranges. We conclude that the variation of O^+ escape as a function of S and K reported here and by Lenn04 are not inconsistent.

We next address the fits to S, K, Q_{EUV}, and I_{EUV} power input levels versus escaping oxygen rates shown on the panels A, B, D, and E of Figure 2. Exponential fits to the data are shown as solid red lines. The exponential fits for S and K show that the observed rate of escaping O^+ increases with increasing incident S and K power.

At Mars, the major escaping ions O^+ and O_2^+ have been reported as a function of S, K, and I_{EUV} by Schnepf et al. (2024) and of I_{EUV} by Dong et al. (2023). The total Mars oxygen mass escape is the sum of the O^+ rate and twice the O_2^+ rate. These values are consistent with other reported rates as a function of other parameters (e.g. Ramstad and Barabash, 2021 and Brain et al. 2017). The variation of escaping oxygen as a function of I_{EUV} from Mars shown in Figure 2D is more than a factor of two smaller than it is from Earth. Direct comparison of Mars and Earth results in panels A, B, and E illustrates that oxygen escape rates from Mars are not as sensitive to variations in the solar power components, S, K, and I_{EUV} as those from Earth.

The exponential fits for solar irradiance power inputs Q_{EUV} and I_{EUV} shown in Figure 2D and E do not completely characterize the variation. At low values of the irradiance power the rate of increase in escaping O^+ is greater per unit of input power than at higher values. These threshold and saturation effects have not been previously reported. Yau et al. (1988) reported an exponential fit for the variation of escaping O^+ as a function of solar power parameterized by the $F_{10.7}$ index. Cully et al. (2003) also reported an exponential fit to the O^+ escape rate as a function of the solar irradiance power index $F_{10.7}$. The full DE 1 data set, not the present one, limited to only the data intervals where observations of S and K are available could provide more insight into the dependence of the O^+ escape rate on solar EUV power.

The weaker response to solar drivers on Mars has been noted by Forbes et al. (2006). They compared the contemporaneous response of Earth's and Mars' thermospheres to the 27-day variation of solar flux parameterized by the $F_{10.7}$ index. Their analysis considered the differences in ionospheric cooling processes in the atmospheres of Mars, Earth, and Venus. They found that the thermospheric temperature response at Mars to variations in $F_{10.7}$ was about half of that at Earth. They also suggested that the thermospheric temperature response of Venus during intervals of enhanced $F_{10.7}$ indices would be less than that of Mars and significantly less than that of Earth.

Oxygen ion escape from Earth is a complex process. The suggestion of different efficiencies of solar irradiance power in driving O^+ escape at low and high levels of irradiance power input at Earth is not unreasonable. The standard model of oxygen energization at Earth involves multiple processes acting from the ionosphere to the plasma sheet (Yau et al. 2021, Peterson et al. 1992, Miyake et al. 1993 and others) to create and provide the 10-eV energy required for an O^+ ion to escape.

4 Summary and Conclusions

It is not yet possible to observationally determine what planetary characteristics (e.g. mass, rotation rate, distance from the star, magnetic field, or atmospheric composition) most strongly influence atmospheric escape or retention. Analysis of similarities and differences in the oxygen escape rates from terrestrial planets as a function of S, K, and Q_{EUV} place new and significant constraints on models of stelar wind/exoplanet interactions and atmospheric escape from exoplanets. We can then use these partially validated models to extend these constraints to the interactions of exoplanet atmospheres to their stelar environments

The magnitude and composition of solar energy inputs to terrestrial atmospheres vary widely. To date only the study of Schnepf et al. (2024) of data from the MAVEN mission to Mars has considered the influence of all components of solar energy input in driving atmospheric escape. This paper extends the observational constrains on the influence of solar drivers of atmospheric escape to Earth by combining observations from DE 1 and IMP 8. The solar drivers include solar irradiance and energy in the solar wind. Here solar wind electrodynamic power (the Poynting flux (S)), solar wind kinetic energy flux (K), and two measures of solar irradiance power Q_{EUV} (0 – 45 nm) and I_{EUV} (0 – 90 nm) are used. The direction of the interplanetary magnetic field was also considered. The results of the re-analysis of observations of escaping O^+ observed on the DE 1 satellite as a function of S, K, and Q_{EUV} were presented in Figure 1C. Differences with a previous analysis by Lenn04 of the dependence of O^+ escape rates on S and K were identified in Figure 2 and discussed.

Lenn04 reported a factor of 2 variation of O^+ escape rates for positive and negative values of IMF B_Z which was confirmed in the reanalysis (Figure 2C).

Lenn04 did not directly compare the influence of solar irradiance on O^+ escape rates because of limited data. Data in Figure 2D and E show that, contrary to the results of prior analysis, the O^+ escape rate is not well characterized by a single exponential increase with increasing solar irradiance. There is a higher rate of increase at low values of Q_{EUV} and I_{EUV} (i.e. a threshold effect).

The data presented above from Earth are compared to the data obtained from Mars by Dong et al. (2023) and Schnepf et al. (2024) in Figure 2. Figure 2 shows that oxygen escape rates from Mars are not as sensitive to the solar power components as those from Earth. Specifically:

- The variation of oxygen escape from Mars as a function of I_{EUV} reported by Dong et al. (2023) is larger than the corresponding variation of escape from Mars as a function of S and K but smaller than that observed at Earth.
- Oxygen escape increases at both Mars and Earth as a function of increasing K but at a significantly reduced rate at Mars.
- O^+ escape at Earth as a function of S appears to have a threshold value of 2×10^{-6} W/m^2 below which the escape rate is constant.

Data exist to extend these comparisons to include Venus (Persson et al. 2020) but have not yet been presented as a function of solar wind Poynting flux (S), kinetic energy flux (K), or solar ionizing radiation.

The data present here demonstrate that the processes most important in driving oxygen escape respond differently to solar drivers on Mars and Earth

Acknowledgements

This research was motivated by our participation in the NASA MACH (Magnetic Fields, Atmospheres, and the Connection to Habitability) DRIVE Science Center (https://mach-center.org/) supported by NASA Grant 80NSSC20K0594. NRS was funded by the NASA MAVEN project through the Mars Exploration Program. AWY acknowledges NSERC Grant RPGIN-2014-06069 and CSA Grant 16SUSTSSPI. WKP thanks Robin Ramstad for helpful conversations and Fazlul Lasker for sharing his informal presentation showing that GOLD neutral temperature determinations are better organized by Q_{EUV} than F_{107}

Open Research

The data used in this investigation were obtained from public data archives. The DE 1 data are described by Peterson (2005) and available from NASA CDAWEB (Candey and Kovolick, 2024). The IMP 8 data from which the S and K indices are described by King and Papitashvili (2004) and Papitashvili and Candey (2024). NASA points to Papitashvili et al. (2020) for access to the data. We found them difficult to find there. We suggest using the data at the NASA web page (2024). The Q_{EUV} and I_{EUV} indices were derived from daily 1 nm resolution solar irradiance spectra obtained from FISM daily 1 hour data page on the LASP Interactive Solar iRadiance Datacenter (2024). The daily 1 nm resolution spectra are described by Chamberlin et al., 2020.

References

Brain, D., S. Barabash, S.W. Bougher, F. Duru, B.M. Jakosky, and R. Modolo (2017), Chapter 15-Solar wind Interaction and atmospheric escape, in The Atmosphere and Climate of Mars, R.M. Haberel, R.T. Clancy, F. Forget, M.D. Smith and R.W. Zurek eds, Cambridge University Press, pp. 464 – 496 DOI: https://doi.org/10.1017/9781139060172.015

Candey, R.M., and T. Kovolick 2024, Coordinated Data Analysis Web (CDAWeb), [Dataset] https://cdaweb.gsfc.nasa.gov/ (Accessed on 26-Feb-2024)

Chamberlin, P. C., F. G. Eparvier, V. Knoer, H. Leise, A. Pankratz, M. Snow, et al. (2020). The flare irradiance spectral model–version 2 (FISM2). *Space Weather*, 18, e2020SW002588. https://doi.org/10.1029/2020SW002588

Cravens, T. E., et al. (2017), Hot oxygen escape from Mars: Simple scaling with solar EUV irradiance, J. Geophys. Res. Space Physics, 122, 1102–1116, doi:10.1002/2016JA023461.

Cully, C. M., Donovan, E. F., Yau, A. W., and Arkos, G. G. (2003), Akebono/Suprathermal Mass Spectrometer observations of low-energy ion outflow: Dependence on magnetic activity and solar wind conditions, J. Geophys. Res., 108, 1093, doi:10.1029/2001JA009200, A2.

Dong, Y., X. Fang, D. A. Brain, J. P. McFadden, J. S. Halekas, J. E. Connerney, S. M. Curry, Y. Harada, J. G. Luhmann, and B. M. Jakosky (2015), Strong plume fluxes at Mars observed by MAVEN: An important planetary ion escape channel Geophys. Res. Lett., 42, 8942–8950, doi:10.1002/2015GL065346

Y. Dong, D.A. Brain, R. Ramstad, X. Fang, J.P. McFadden, J.S. Halekas, F. Eparvier, J.R. Espley, J.R. Gruesbeck, B.M. Jakosky, (2023), The dependence of Martian ion escape on solar EUV irradiance as observed by MAVEN, Icarus, 393, 115288, https://doi.org/10.1016/j.icarus.2022.115288.

Feldman, W. C., J.R. Asbridge, S.J. Bame, S. J., and J.T. Gosling, (1978), Long-term variations of selected solar wind properties: Imp 6, 7, and 8 results, *J. Geophys. Res.*, 83(A5), 2177–2189, doi:10.1029/JA083iA05p02177.

FISM daily 1 hour data page on the LASP Interactive Solar iRadiance Datacenter (2024), [Dataset] https://lasp.colorado.edu/eve/data_access/eve_data/fism/daily_hr_data/ (Accessed on 26-Feb-2024)

Forbes, J.M., S. Bruinsma, and F. G. Lemoine (2006), Solar Rotation Effects on the Thermospheres of Mars and Earth, Science, 312, 1366-1368, https://www.science.org/doi/epdf/10.1126/science.1126389

Gunell, H., et al. (2018), Why an intrinsic magnetic field does not protect a planet from atmospheric escape, A&A, doi:10.1051/0004-6361/201832934

Hoffman, R.A. and E.R. Schmerling (1981), Dynamics Explorer program: An Overview, Space Sci. Instrumentation, 5 345-348.

King, J.H. and N.E. Papitashvili (2004), Solar wind spatial scales in and comparisons of hourly Wind and ACE plasma and magnetic field data, J. Geophys. Res., Vol. 110, No. A2, A02209, https://doi.org/10.1029/2004JA010649

Maggiolo, R., L. Maes, G. Cessateur, F. Darrouzet, J. De Keyser, J., & H. Gunell, (2022). The Earth's magnetic field enhances solar energy deposition in the upper atmosphere.

Journal of Geophysical Research: Space Physics, 127, e2022JA030899. https://doi.org/10.1029/2022JA030899
Miyake, W., T. Mukai, and N. Kaya (1993), On the evolution of ion conics along the field line from EXOS D observations, *J. Geophys. Res.*, 98(A7), 11127–11134, doi:10.1029/92JA00716.
NASA web page, 2024, Yearly omni2 data [Dataset] https://spdf.gsfc.nasa.gov/pub/data/omni/low_res_omni/ (Accessed on 26-Feb-2024)
Lennartsson, O.W., H.L. Collin, and W.K. Peterson (2004), Solar wind control of Earth's H^+ and O^+ outflow in the 15-eV to 33-keV energy range, J. Geophys. Res., 109, A12212, doi:10.1029/2004JA010690.
Lockwood, M. (2019). Does adding solar wind Poynting flux improve the optimum solar wind-magnetosphere coupling function? Journal of Geophysical Research: Space Physics, 124, 5498– 5515. https://doi.org/10.1029/2019JA026639
Meier R. R., et al. (2015) Remote Sensing of Earth's Limb by TIMED/GUVI: Retrieval of thermospheric composition and temperature, Earth and Space Science, 2, 1–37, doi: 10.1002/ 2014EA000035.
Papitashvili, Natalia E. and King, Joseph H. (2020), "OMNI Hourly Data" [Data Set] https://doi.org/10.48322/1shr-ht18, (Accessed on on 26-Feb-2024)
Papitashvili, N, and R. Caney, (2024), The Low Resolution OMNI data set, OMNI (LRO), [Datset] https://omniweb.gsfc.nasa.gov/html/ow_data.html Accessed on 26-Feb-2024)
Persson, M., Y. Futaana, R. Ramstad, K. ,Masunaga, H. Nilsson, M. Hamrin, et al. (2020). The Venusian atmospheric oxygen ion escape: Extrapolation to the early solar system. Journal of Geophysical Research: Planets,125, e2019JE006336. https://doi.org/10.1029/2019JE006336
Peterson, W.K., H.L. Collin, M.F. Doherty, and C.M. Bjorklund (1992) O^+ and He^+ Restricted and Extended (Bi-Modal) Ion Conic Distributions, Geophys. Res. Lett., 19, 1439, 1992.
Peterson, W.K, (2005), The Energetic Ion Mass Spectrometer data description, [Dataset] https://lasp.colorado.edu/timas/info/DE/DE_eics_home.html (Accessed on 26-Feb-2024)
Peterson, W. K., H. L. Collin, O. W. Lennartsson, and A. W. Yau (2006), Quiet time solar illumination effects on the fluxes and characteristic energies of ionospheric outflow, J. Geophys. Res., 111, A11S05, doi:10.1029/2005JA011596.
Peterson, W. K., L. Andersson, B. C. Callahan, H. L. Collin, J. D. Scudder, and A. W. Yau (2008), Solar-minimum quiet time ion energization and outflow in dynamic boundary related coordinates, J. Geophys. Res., 113, A07222, doi:10.1029/2008JA013059.
Ramstad, R. and S. Barabash, (2021), Do Intrinsic Magnetic Fields Protect Planetary Atmospheres from Stellar Winds? Space Sci Rev 217, 36. https://doi.org/10.1007/s11214-021-00791-1
Rodríguez-Zuluaga, J., Stolle, C., Hysell, D. et al. Topside equatorial spread F-related field-aligned Poynting flux: observations and simulations. Earth Planets Space 74, 119 (2022). https://doi.org/10.1186/s40623-022-01679-2
Shelley, E.G., D.A. Simpson, T.C. Sanders, E. Hertzberg, H. Balsiger, and A. Ghielmetti (1981), The energetic ion composition spectrometer (EICS) for the Dynamics Explorer-A, Space Sci. Instrumentation, 5, 443-454.

Schillings et al. Earth, Planets and Space (2019) 71:70 https://doi.org/10.1186/s40623-019-1048-0

Shizgal, B.D. and G.G. Argos (1996), Nonthermal escape of the atmospheres of Venus, Earth, and Mars, Rev of Geophysics, 34, 4. pages 483-505, https://doi.org/10.1029/96RG02213

Schnepf, Neesha Regmi, Yaxue Dong, David Andrew Brain, et al. (2024), Solar and solar wind energy drivers for O^+ and $O2^+$ ion escape at Mars. *ESS Open Archive* . February 23, 2024. DOI: 10.22541/essoar.170870888.88593189/v1

Schonfeld, S.J., S.M. White, C.J. Henry, C.N. Arge, and R.T.J. McAteer (2015), Coroal sources of the solar $F_{10.7}$ radio flux, Ap. J. 808:29, doi:10.1088/0004-637X/808/1/29

Schonfeld, S.J., S.M. White, R.A. Hock-Mysliwiec, and R.R.J. McAteer (2017), The slowly varying corona. 1. Daily differential emission measure distributions derived from EVE spectra, Ap.J. 844:163, doi: 10.3847/1538-4357/aa7b35

Strangeway, R. J., Ergun, R. E., Su, Y.-J., Carlson, C. W., and Elphic, R. C. (2005), Factors controlling ionospheric outflows as observed at intermediate altitudes, J. Geophys. Res., 110, A03221, doi:10.1029/2004JA010829.

Strangeway, R. J., C.T. Russell, J.G. Luhmann, T.E. Moore, J.C. Foster, S.V. Barabash, and H. Nilsson, (2010) Does a Planetary-Scale Magnetic Field Enhance or Inhibit Ionospheric Plasma Outflows?, American Geophysical Union, Fall Meeting 2010, abstract id.SM33B-1893

Strangeway, R.J., C.T. Russell, J.G. Juhmann, T.E. Moore, and S.V. Barabash (2019), A Planetary-Scale Magnetic Field Can Enhance, rather than Inhibit, Ionospheric Escape, Abstract SM52B-05 presented at the 2019 AGU Fall Meeting, 9-13 Dec.

Strickland, D. J., J.S. Evans, and L.J. Paxton, (1995), Satellite remote sensing of thermospheric O/N_2 and solar EUV: 1. Theory, J. Geophys. Res., 100(A7), 12217–12226, doi:10.1029/95JA00574.

Strickland, D.J., J.L. Lean, R.R. Meier, A.B. Christensen, L.J. Paxton, D. Morrison, J.D. Craven, R.L. Walterscheid, D.L. Judge, and D.R. McMullin (2004), Geophys. Res. Lett., 31, L03801, doi:10.1029/2003GL018415.

Welling, D.T., M. André, I. Dandouras et al. The Earth: Plasma Sources, Losses, and Transport Processes. Space Sci Rev 192, 145–208 (2015). https://doi.org/10.1007/s11214-015-0187-2

Yau, A. W., P.H. Beckwith, W.K. Peterson, and E.G. Shelley, (1985), Long-term (solar cycle) and seasonal variations of upflowing ionospheric ion events at DE 1 altitudes, J. Geophys. Res., 90(A7), 6395– 6407, doi:10.1029/JA090iA07p06395.

Yau, A. W., W. K. Peterson, and E. G. Shelley (1988), Quantitative parameterization of energetic ionospheric ion outflow, in Modeling Magnetospheric Plasma, Geophysical Monograph 44, T. E. Moore and J. H. Waite, Jr., Eds., Amer. Geophys. U., Washington, D.C., p. 211.

Yau, A.W., T. Abe, M. André, A.D. Howarth, and W.K. Peterson (2021), Ionospheric ion acceleration and transport, in Space Physics and Aeronomy Collection Volume 2: Magnetospheres in the Solar System, Geophysical Monograph 259, First Edition. Edited by Romain Maggiolo, Nicolas André, Hiroshi Hasegawa, and Daniel T. Welling. © 2021 American Geophysical Union. DOI: 10.1002/9781119507512